Far East Journal of Electronics and Communications

http://www.pphmj.com
http://dx.doi.org/10.17654/EC017020327
Volume 17, Number 2, 2017, Pages 327-349 **ISSN: 0973-7006**

MECHANICAL DEVICE WITH FIVE-ARMS TESTED ON SERVICE

G. Caligiana, A. Liverani, D. Francia and L. Frizziero

Department of Industrial Engineering
Alma Mater Studiorum University of Bologna
Viale Risorgimento, 2 - I-40136, Bologna, Italy

Abstract

We present the stress analysis of a pouring concrete device. In order to test the prototype of a pouring concrete equipment composed of five-arms with hollow rectangular cross sections, an extensive study about equipment for pouring concrete has been undertaken. An upgrade of a four-arms device already existing and actually working would be developed. Tests have been performed both on the prototype of the equipment and on a virtual model of the device, performed by a 3D CAD modeler and analyzed through FEM numerical programs. During experimental tests, a laser device has measured deflections at the end of the fifth arm, corresponding to applied loads. For measuring strains in the critical points highlighted by the numerical simulation strain rosette have been employed. In both the static and the dynamic conditions, Mohr's circles have been drawn from the 3D strain state and the 2D plane stress experimental records and they have been compared with those predicted through the finite element analysis. From the comparison between numerical and experimental results, a very good correlation has been obtained for static loading to assess the soundness of the virtual model.

Received: October 10, 2016; Accepted: January 20, 2017
Keywords and phrases: Mohr's circle, CAD, FEM, articulated device, strain analysis.

Nomenclature

$\varepsilon_1 =$	corrected strain in the direction 1
$\varepsilon_2 =$	corrected strain in the direction 2
$\varepsilon_3 =$	corrected strain in the direction 3
$\hat{\varepsilon}_1 =$	uncorrected strain in the direction 1
$\hat{\varepsilon}_2 =$	uncorrected strain in the direction 2
$\hat{\varepsilon}_3 =$	uncorrected strain in the direction 3
$\nu_0 =$	Poisson's ratio
$\phi =$	principal angle
$K_1 =$	transverse sensitivity coefficient in the direction 1
$K_2 =$	transverse sensitivity coefficient in the direction 2
$K_3 =$	transverse sensitivity coefficient in the direction 3
$\varepsilon_{pI} = I$	in-plane principal strain
$\varepsilon_{pII} = II$	in-plane principal strain
$E =$	Young's modulus
$\sigma_{pI} = I$	principal stress.

1. Introduction

Experimental stress analysis is commonly aimed to determine the significant stresses in a test object as accurately as necessary to assure product reliability under expected service conditions. However, stress analysis, even of simple geometries, can lead to complicated mathematical operations. Some industrial products, such as engine crankshafts, medical prostheses, moving machines parts have boundary shapes that cannot be

easily described mathematically. The experimental approach, which is based on the construction of a physical prototype, reveals the stresses in a measurable way. The nature of forces and stresses cannot be measured directly. It is the effect of a force that is measurable: experimental stress analysis, then, is actually experimental strain analysis.

In the industrial field static and dynamical loads applied on structures of different shape, dimension and material are the principal extents to be investigated to ensure the structural resistance under operational conditions. The most interested domains in this kind of investigation are the constructions of buildings, dams, bridges, roadways.

This paper presents an accurate stress analysis of a pouring concrete device. Concrete pouring is a conventional activity to obtain foundations, beams, building slabs, well-drained bases to support heavy loads like vehicles. Often these operations have to be performed in limited and constrained space, so transportable devices become necessary to reach all significant sites.

An extensive study about equipment for pouring concrete has been undertaken at DIEM Department (now named DIN-Department of Industrial Engineering) [1]. A company in the Romagna countryside charged our research group to test a prototype of a pouring concrete device, shown in Figure 1, composed of five-arms with hollow rectangular cross sections.

Figure 1. The five-arms prototype.

Both a simulated analysis through FEM (finite element analysis), in order to prevent the worst working conditions, and an experimental analysis, in order to test the structure at a deep grade of accuracy, have been performed.

A complete CAD (computer aided design) activity has been undertaken to model the pouring device for the simulation, leading to reliable virtual models for further finite element analysis.

This approach ensures a good validity to verify the behavior of the mechanical set, to validate the numerical calculation methodology and to verify the deviation of the numerical results with the reality. Furthermore, a previous design and optimization process, using numerical technologies first, and the extensiometric procedures then, allows to check the numerical results and the methodology of design [2].

For the experimental analysis rectangular rosettes have been instrumented on the real prototype to verify its behavior under loading conditions. In the case of the general biaxial stress state, with the principal directions unknown, three independent strain measurements in different directions are required to determine the principal strains and stresses; even when the principal directions are known in advance, two independent strain measurements are needed to obtain the principal strains and stresses. The biaxial stress state occurs very commonly in machine parts and structural members, so the strain gages used in experimental stress analysis would be rosettes. The selection and application of rosettes is critical to their successful use in experimental stress analysis and the ability in the location and the accuracy of the system layout to read the results is a need.

This paper presents a sequential methodology to examine the apparatus first by numerical test and finally to validate the results by experimental tests. As the common practice in structural analysis suggests, [3, A], the virtual modeling and simulation of the equipment have been performed first, aimed to highlight the most critical areas, then the equipment has been charged by both static and dynamic loadings, to record the strains in the critical investigated areas, thus allowing to map the real stresses that work on the

equipment. Figure 2 shows the sequence that describes the approach from virtual analysis to experimental tests.

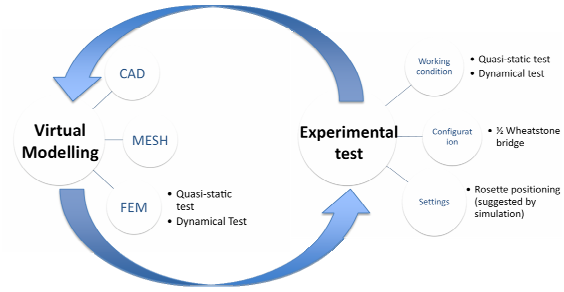

Figure 2. The sequence of analysis.

2. Materials and Method

2.1. The pouring concrete device prototype

The equipment consists of beams of Weldox 900 E steel (S890QL) [5], with hollow rectangular cross sections. The principal mechanical properties of this steel are collected in Tables 1-3.

Table 1. Weldox 900E (S890QL) steel-chemical composition

	Max %
C*	0,20
Si*	0,50
Mn*	1,60
P	0,020
S	0,010
B*	0,005
Nb*	0,04
Cr*	0,70
V	0,06
Cu	0,10
Ti*	0,04
Al* total	0,018
Mo*	0,70
Ni	0,10
N	0,015

*Intentional alloying elements. The steel is grain-refined.

Table 2. Weldox 900E (S890QL) steel-mechanical properties: tests performed on transverse test pieces

Plate thickness (mm)	Yield strength $R_{p0,2}$ (min.) (MPa)	Tensile strength R_m (MPa)	Elongation A_5 (min.) (%)
4,0-50,0	900	940-1100	12
50,1-80,0	830	880-1100	12

Table 3. Weldox 900E (S890QL) steel-impact properties: tests performed on transverse Charpy $V10 \times 10$ test specimens

Test temperatures (°C)	Impact energy (J)
0	35
-20	30
-40	27

Table 3 summarizes the steel properties resulting from transverse impact testing according to EN 10025, option 30, on sub-size Charpy *V*-specimens are used for plate thickness less than 12 mm: the specified minimum value is then proportional to the cross section of the specimen. The fully extended configuration of the equipment is 58-meter long. Each arm is pin-joined to the preceding one. Hydraulic cylinders allow relative motion of each of the five-arms with respect to the adjoining one. Each arm is suitably shaped and, at rest, it can be folded upon the preceding one, resulting in a whole assembly, which can be carried by a suitable tractor unit. External and internal height and width of the cross sections are often different for different locations, because arms are suitably shaped to allow the assemblage of the folded configuration for transportation and because they are dimensioned by roughly following the theory of a beam of uniform strength in bending. Obviously, economical reasons do not suggest a continuous change in dimensions, but rather a proper discrete change in thickness in several regions, made, for example, by applying reinforcement slabs welded in suitable locations, chosen by the designer. In the paper, the arms of the equipment have been numbered with roman numbers, starting from the first arm.

2.2. The virtual model

The numerical 3D model of the prototype has been implemented by CAD software. The virtual model activity consists in the design of each arm of the device, progressively numbered starting from the arm nearest to the tractor unit, paying attention to remove clearances, interferences or shape imperfections [6]. The principal aim is to avoid bugs or malfunctions during successive finite element analysis. A proper simulation is needed to reproduce the mutual actions between arms, by means of hydraulic rams and appropriate constraints on the contact surfaces [1]. Virtual models have been imported inside FEM software environment (MD Patran, R2.1, and MD Nastran, R3) to perform finite element analysis [7-10]. During the first rough automatic meshing, ten-node tetrahedral isoparametric elements have been utilized. The complex geometry of the structure required a local mesh refinement in peculiar regions and a proper set-up to ascertain mesh fine-tuning and element shape quality. Convergence tests have been performed to assess the achievement of a reliable solution. In a more suitable re-arrangement of the geometric model a mesh with four-node, bilinear thick-shell elements has been implemented: for instance, a solution achieved in static conditions for the fifth arm, with a mesh of 74890 shell elements, where the main element has a length of 10 mm, needs a computation time of 1165 seconds. This is the total time needed for mesh input data, stiffness matrix assembling, constraint settling, equation system solution and output file creation. For the same element a solution with a mesh of 19655 shell elements, with main element length of 20 mm, needs a computation time of 35 seconds, whereas a solution with a mesh of 6162 shell elements, with main element length of 40 mm, needs a computation time of 10 seconds. Structural loads due to arm’s own weight have been applied in the centre of mass of each section. This item is comprehensive of accessories and welds, which have been estimated to constitute about 7% of the total mass. The resultant forces of structural loads due to the piping system to pour concrete, with the weight of concrete added up, have been applied in the suitable points of the structure, where ducts are actually joined. The mass of all link devices to allow arm movements have been considered. In static tests, each

arm has been considered by itself and the actions applied by other arms are properly calculated [1]. This task has been performed by starting from the last arm (arm V) and then coming backwards to the first one (arm I). Figure 3 shows the scheme of loads and reactions applied to the fifth arm.

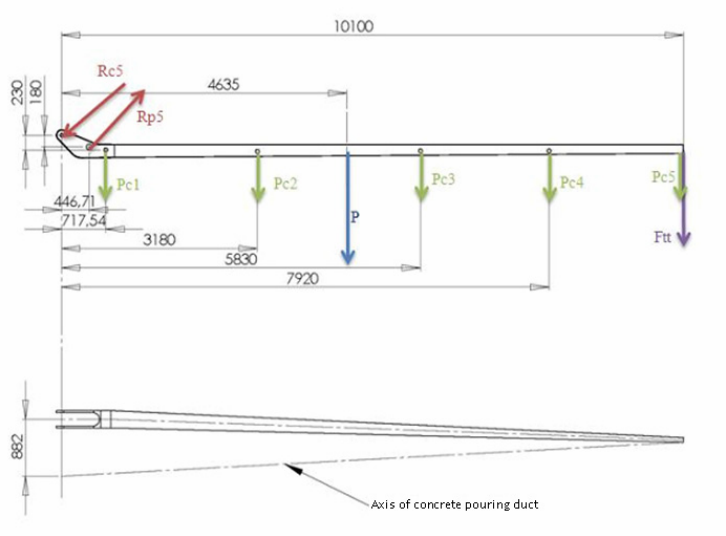

Figure 3. Scheme of loadings and reactions applied to arm *V*.

Virtual probes have been located on the FEM model to derive stress and strain values in the same locations where rectangular strain rosettes on the prototype have to record experimental results. Figure 4 shows the location of the rosettes on each arm.

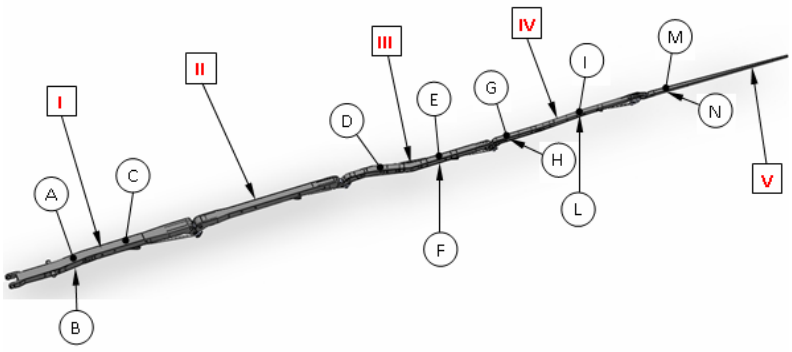

Figure 4. The location of twelve rectangular rosettes on the five-arms device.

2.3. The experimental device

Rosettes are designed to perform a very practical and important function in experimental stress analysis.

It is known that, for the general biaxial stress state with the principal directions unknown, three independent strain measurements are required to determine the principal strains and stresses.

Even when the principal directions are known in advance, two independent strain measurements are needed to obtain the principal strains and stresses. To meet these requirements, three basic types of strain gage rosettes are manufactured: the Tee rosette, with two mutually perpendicular grids, 0-90 degree, the Rectangular rosette, with three grids, with the second and third grids angularly displaced from the first grid by 45 degrees and 90 degrees, respectively and the Delta rosette, with three grids too, with the second and third grids 60 degrees and 120 degrees away, respectively, from the first grid.

In our case the directions of the principal strains are unknown, so a three-element rectangular rosette is required.

The principal disadvantage of this kind of rosette arises from transverse sensitivity error when performing rosette data reduction [11]. The magnitude of the error in any particular case depends on the transverse sensitivity coefficient.

Moreover, when strain measurements must be made in a variable thermal environment, the thermal output of the strain gage can produce rather large errors so there is the need to zero-balanced the instrumentation at the testing temperature, under strain-free conditions. Under load, three strain values are recorded at each load increment: as follows, these raw strain readings are designated as '$\wedge$' because they are uncorrected strain. These strain readings have been corrected for the transverse loading of the gage in a rectangular rosette, as the following equations summarize [12]:

$$\varepsilon_1 = \frac{\hat{\varepsilon}_1 \cdot (1 - \nu_0 K_1) - K_1 \hat{\varepsilon}_3 \cdot (1 - \nu_0 K_3)}{1 - K_1 K_3}, \tag{1}$$

$$\varepsilon_2 = \frac{\hat{\varepsilon}_2 \cdot (1 - \nu_0 K_2)}{1 - K_2} - \frac{K_2 \cdot [\hat{\varepsilon}_1 \cdot (1 - \nu_0 K_1) \cdot (1 - K_3) + \hat{\varepsilon}_3 \cdot (1 - \nu_0 K_3) \cdot (1 - K_1)]}{(1 - K_1 K_3) \cdot (1 - K_2)}, \quad (2)$$

$$\varepsilon_3 = \frac{\hat{\varepsilon}_3 \cdot (1 - \nu_0 K_3) - K_3 \hat{\varepsilon}_1 \cdot (1 - \nu_0 K_1)}{1 - K_1 K_3}. \quad (3)$$

The transverse sensitivity coefficients K1, K2, K3 are given in the manufacturer's data sheet. The equations to calculate the two principal strains from the corrected strains are described as follows:

$$\varepsilon_{pI} = \frac{1}{2} \cdot (\varepsilon_1 + \varepsilon_3) + \frac{1}{2} \cdot \sqrt{(\varepsilon_1 - \varepsilon_3)^2 + (2 \cdot \varepsilon_2 - \varepsilon_1 - \varepsilon_3)^2}, \quad (4)$$

$$\varepsilon_{pII} = \frac{1}{2} \cdot (\varepsilon_1 + \varepsilon_3) - \frac{1}{2} \cdot \sqrt{(\varepsilon_1 - \varepsilon_3)^2 + (2 \cdot \varepsilon_2 - \varepsilon_1 - \varepsilon_3)^2}. \quad (5)$$

The principal angle ϕ is given by equation (6), as follows:

$$\tan 2\phi = \frac{2 \cdot \varepsilon_2 - \varepsilon_1 - \varepsilon_3}{\varepsilon_1 - \varepsilon_3}. \quad (6)$$

The principal stresses computed from the corrected strains for a linear, isotropic and homogeneous material are:

$$\sigma_{pI} = E\left[\frac{(\varepsilon_1 + \varepsilon_3)}{2 \cdot (1 - \nu_0)} + \frac{1}{2 \cdot (1 + \nu_0)} \cdot \sqrt{(\varepsilon_1 - \varepsilon_3)^2 + (2 \cdot \varepsilon_2 - \varepsilon_1 - \varepsilon_3)^2}\right], \quad (7)$$

$$\sigma_{pII} = E\left[\frac{(\varepsilon_1 + \varepsilon_3)}{2 \cdot (1 - \nu_0)} - \frac{1}{2 \cdot (1 + \nu_0)} \cdot \sqrt{(\varepsilon_1 - \varepsilon_3)^2 + (2 \cdot \varepsilon_2 - \varepsilon_1 - \varepsilon_3)^2}\right], \quad (8)$$

$$\sigma_{pIII} = 0. \quad (9)$$

To test the pouring concrete device, twelve rectangular rosettes have been glued in suitable sites, as shown in Figure 4, chosen on the basis of FEM preliminary results. Rosettes have three strain gages at 0°, 45° and 90°. Attention has been paid to align the central strain grid (gage 2 at 45°) along

the beam symmetry axes of each arm. In the set-up the strain rectangular rosettes have been generally located in the upper and lower surfaces of the beam of each arm (the areas farther from the neutral axes), being the main loading in the whole structure due to bending [12].

As a consequence, *A* and *C* rosettes have been located in suitable sites in the upper surface of arm I, while *B* rosette has been placed on the lower surface of arm I. Arm III is in the middle of the equipment, so it has been shaped according to a curved geometry much more than the others, to allow the folding operation before any transportation of the whole articulated device. Owing to its peculiar contour, strain recording in some areas of the third arm is strongly recommended. *D* and *E* rosettes have been located in the upper surface of arm III and *F* rosette on its lower face. Arms IV and V have progressively smaller sections and they have some stress and strain raisers. *G* and I rosettes have been put on the upper surface of arm IV; *H* and *L*, respectively, on the lateral and lower surface of arm IV. *M* rosette has been located on the upper surface of arm *V* and *N* rosette on its lateral surface. Whenever critical areas have been chosen, suitable distance from extreme strain raisers has been maintained to let sufficient reliability for all rosette strain readings.

2.4. Experimental tests

Experimental results have been recorded by an eight channel Esam Traveller plus device [13]. Each strain gage of each rectangular rosette is connected through an half Wheatstone bridge to the corresponding strain gage of the rosette used for temperature compensation. Full Wheatstone bridge has been obtained by suitably connecting the half bridge to the Esam Traveller device circuits. Thus, bridge balancing and successive recordings of the experimental information can be performed. Results have been elaborated through the resident device but, owing to some deficiencies in the native program, “ad hoc” numerical modules have been written by one of the authors in Mathematica® language, R6. Some of the final output of the numerical program are 3D Mohr circles, which very efficiently visualize

static and dynamic situations of each measurement section [14]. Preliminary quasi-static tests have been performed on the prototype of the articulated device, in its extended configuration. Discrete known loads, measured by a dynamometer (60 kg ≈ 588 N, 90 kg ≈ 883 N, 120 kg ≈ 1177 N, 150 kg ≈ 1471 N, 180 kg ≈ 1765 N), have been applied at the end of the fifth arm of the structure. Deflections at the end of the last (fifth) arm, corresponding to each applied load, have been measured by a laser device (positive values correspond to downward deflections, Figure 5).

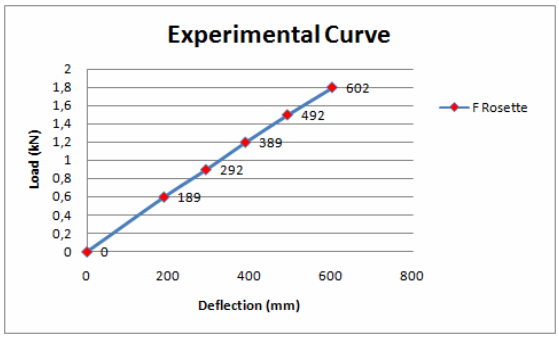

Figure 5. Quasi-static tests: experimental load-versus-deflection curve measured at the end of the fifth arm.

In each site where rectangular rosettes are present, the 2D plane stress state and the 3D strain state can be derived. Principal stresses, principal strains, directions of the principle strains and stress, Mohr stress and strain circles have been recorded and compared with those predicted through the finite element analysis. Figure 6 shows for explanatory purpose, the 2D plane stress state relative to the "*L*" rosette glued on the fourth arm: the axis in red corresponds to the *x*-axis, the direction of the strain gage 1 of rosette "*L*", while blue axis is the direction of the y-axis, the direction of the strain gage 3 of rosette "*L*". Obviously, the two orthogonal axes results, as expected, at 180° inside the Mohr circle.

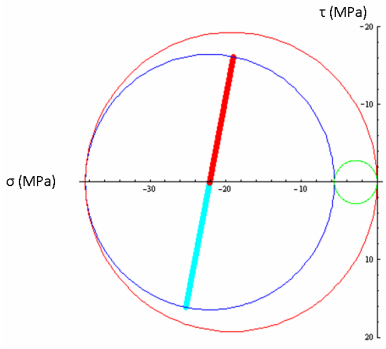

Figure 6. Quasi-static tests: Mohr stress circle obtained by results from "*L*" rectangular strain gage rosette during quasi-static tests.

A second plan of dynamical tests has been performed, by simulating pouring of concrete. Two (medium and high) pumping frequencies are considered: 22 strokes/min (0,37 Hz, corresponding roughly to 125 m3/h) and 26 strokes/min (0,43 Hz, corresponding roughly to 150 m3/h). Pseudo random strain histories can be recorded by rectangular rosettes, as shown in Figure 7.

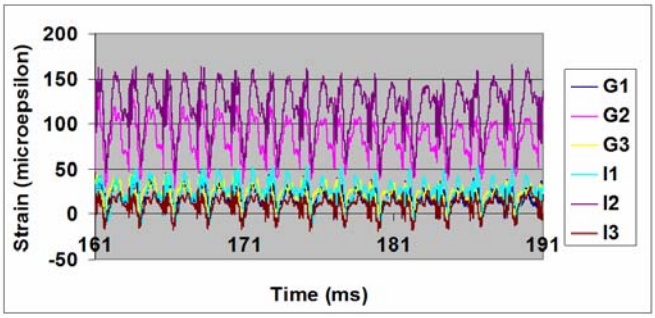

Figure 7. Strain histories recorded by each strain gage of "*G*" and "*I*" rosettes during simulated dynamic condition at maximum pumping frequency.

Actually, histories show almost periodic peaks of similar amplitude (even if not exactly identical one to each other) at correspondingly analogous intervals of time. Experimental results lead to the knowledge of stresses, strains, principal directions and Mohr circles as a function of time. Inside the

pseudo random history, accurate study of stress and strain circles of maximum diameter (normally corresponding or very near to a maximum of the strain history), testifies, as expected, that dynamical actions are much more critical for the structure than static ones. The frequency response (resonance) of the structure to the action of the pumping frequencies seems very important for structure strength as testified by experimental tests and confirmed by finite element analysis.

2.5. From numerical prediction to experimental tests

Principal stresses, principal strains, directions of the principle strains and stresses, Mohr stress and strain circles have been recorded and compared with those predicted through the finite element analysis. FEM results evidenced in all cases that stresses recorded numerically are almost everywhere well below the yield strength of the material and strains are entirely within the elastic field. Owing to the linearity of the problem, the maximum weight hanged up, during static experimental tests, at the end of the fifth arm, has been considered directly in the analysis of the quasi-static condition. Moreover, the maximum value of 1765 N (≈ 180 kg) corresponds roughly to the weight of the ending part of the duct for pouring concrete, completely filled with concrete. On the experimental counterpart, strain rosettes have been glued on the apparatus already assembled. So, Wheatstone bridge circuit of the rosette strain gages has been balanced to zero, while structural loadings were obviously already on. Low strain condition could allow the application of the superposition principle. Nevertheless, to avoid the suspect of geometrical nonlinearities, an analysis of the displacements must be considered. Resulting deflections are significant, but completely negligible if compared to the length of the arms or of the whole structure (58 meters). Once and for all, two FEM program runs have been performed for the fifth arm, to ascertain the lack of geometric nonlinearities: the former with both structural and external loadings (of 1765 N), the latter with only structural loadings. The difference between them represents the situation of the application of external loadings to an already deformed structure (identical to the experimental one). This result has been compared to a FEM

run performed by simply applying the only external loading to the original frame. Comparison is not shown here, but it leads to almost coincident results, testifying the uselessness of the previous much more involved analysis. So, in the FEM analyses of all the consecutive arms, static test external loading has been applied to the end of the fifth arm, simply ignoring the frame structural loads. Comparison has been made on terms of principal stress and strain values, direction of principal stresses and strains, equivalent stress and strain values. An impressive compendium of the comparison between numerical predictions and experimental results through Mohr circles can be seen in Figure 8 for the "*C*" rosette on the third arm.

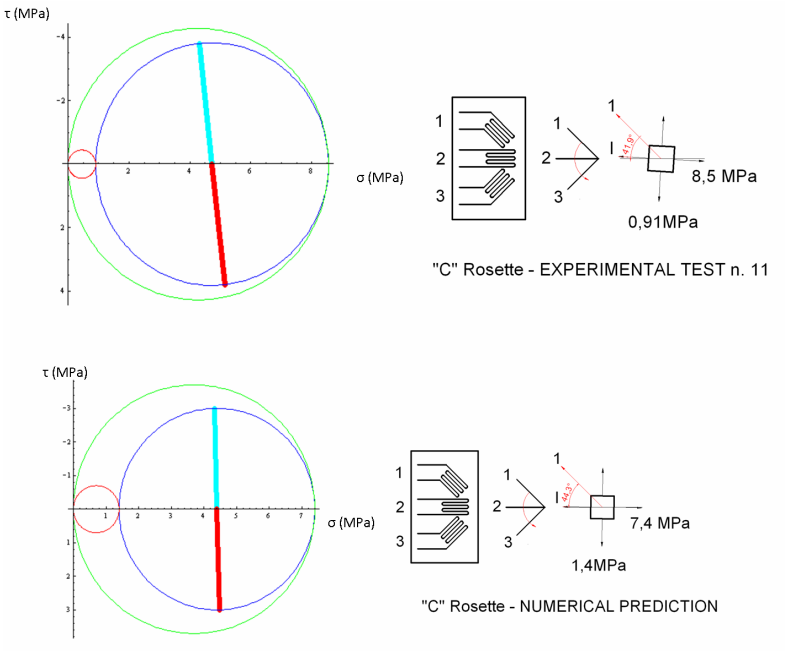

Figure 8. The stress Mohr circle and principal stress directions experimentally and numerically obtained, respectively, for rosette "*C*".

In Figure 9, the boundary conditions and the loads on the fifth arm are displayed: a hinge constraint on the first hole on the left allows the rotation along the hole axis; the second inner hole has been constrained through a fixed constraint, the right extreme of the arm has been charged by a load of

180 kg about. FEM results for the fifth arm have been obtained with a shell element meshing, in quasi-static conditions, with an applied loading at the end of the fifth arm of 1765 N. In Table 4, the main experimental and numerical values derived from the analysis are listed: in particular the principal strains and stresses and the principal angle have been calculated through the Mohr's circle analysis, as above described. The equivalent strain and the equivalent von Mises stresses have been compared facing the experimental values to the numerical prediction. In Table 4, only the values referred to the fifth arm are displayed in order to show the most critical condition on the device. In fact the fifth arm is the one directly put under the concrete pouring load (1765 N): once applied on the arm, the extensiometric rosette estimated only the strains due to this load and not those due to the structural load. Thus, the experimental values have been compared to the numerical values obtained from the total FEM results (structural load plus 1765 N) minus the results obtained only from the structural FEM analysis. In Table 4, the values to be compared are referred as experimental value and numerical prediction. Table 5 shows the evaluation for rosettes *M* and *N* of how the numerical prediction moves away from the experimental value: the maximum error lies under 10%, thus confirming the validity of the methodology adopted.

Further analysis, not proved in this paper, evidenced the influence of the weight of the fifth arm on the whole device structure. A huge weight reduction of the entire device has been observed, strictly depending on the only 25% lightening of the fifth arm by means of optimized design, lattice structures and the employment of advanced materials.

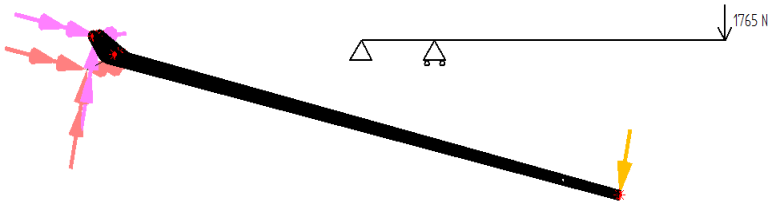

Figure 9. The boundary conditions on the fifth arm.

Table 4. The experimental and numerical values comparison for principal and equivalent stresses and strains

	Experimental value		FEM (structural load)		FEM (structural load + 1765N)		Numerical prediction	
	M	*N*	*M*	*N*	*M*	*N*	*M*	*N*
Principal strain $\varepsilon_{pI}(\mu\varepsilon)$	220	30,9	283,8	55,4	427,3	72,2	143,5	16,8
Principal strain $\varepsilon_{pII}(\mu\varepsilon)$	-36,7	18,7	-171,9	-75,1	-258,6	-103,9	-86,7	-28,8
Principal stress $\sigma_{pI}(MPa)$	43,8	8,4	57	2,2	102,7	2,8	45,7	0,6
Principal stress $\sigma_{pII}(MPa)$	6,79	6,5	10,6	-6,2	19,1	-14,2	8,5	-8
Principal angle (degree)	44,2	87,5	-	-	-	-	45,9	69,2
Equivalent strain $(\mu\varepsilon)$	216	36,4	319,6	48,4	481,2	68,3	161,6	19,9
Equivalent von Mises stress (MPa)	45,3	7,6	52,5	9,7	94,6	13,7	42,1	8,3

Table 5. The error calculated between the numerical prediction and the experimental value for rosettes *M* and *N*

Rosette	Experimental value	Numerical prediction	Error (%)
M	45,3	42,1	7
N	7,6	8,3	8

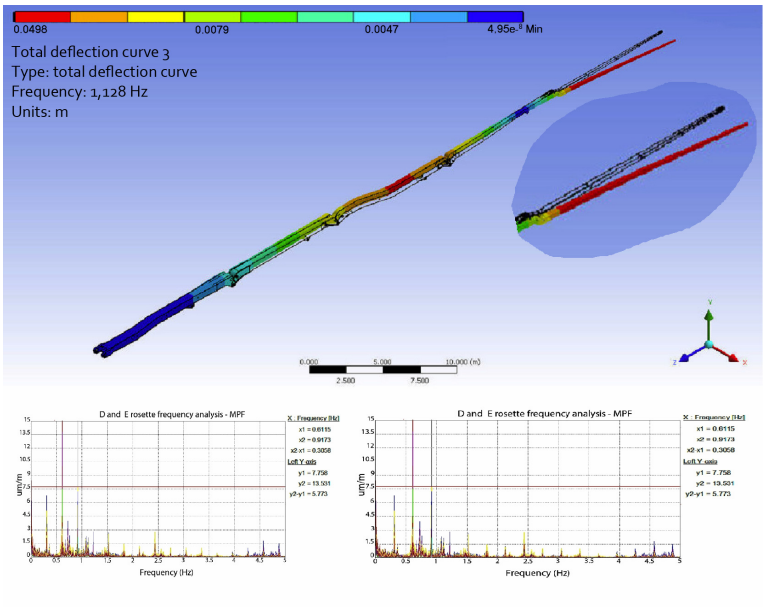

Figure 10. The critical deflection at the root of the fifth arm and the frequencies analysis results on the fifth and third arm, respectively.

Convergence analysis has been performed to verify the soundness of finite element mesh, by using numerical predictions for quasi-static tests. Three different mesh refinements have been considered: a first meshing has been obtained automatically, suggested by the software default settings. Further refinements underlined that a reduction of almost 1/3 in element size results when going to most accurate meshing, with increasing elements number and consequent increasing computational time. Numerical predictions show how a sufficiently accurate mesh refinement allows stress and strain results to converge towards experimental results, testifying the accuracy of FEM virtual modeling. Results shown in this paper have been obtained by a compromise solution in terms of accuracy and computational time. As above mentioned, strain rosettes have been glued on the equipment already deformed by its structural loadings and, in this condition, Wheatstone bridge circuit has been balanced. To ensure comparable configurations for experimental and numerical analyses, two finite element program runs have been performed, the former with only structural loadings (and without

external loadings), the latter with both structural and external loadings applied during dynamical experimental tests. Accounting to the superposition principle, the outcome resulting from the difference between the second and the first FEM runs is considered as the numerical prediction to be directly compared with the experimental results. This approach is particularly useful in the modal analysis performed during the modeling of the dynamical concrete pouring loading. Starting from the knowledge of the mass flow rate of concrete and from the number of strokes per minute at two different working regimes (medium and high), motion equations have been settled to obtain axial forces transferred by friction to the duct of concrete and, consequently, to the device. Dynamic loadings have been properly added to the structural ones and a single virtual model of the whole structure has been implemented, instead of several models for each arm, as in the quasi-static analysis. Actually, the presence of alternating forces implies oscillating reactions too, to be exchanged between arms; so, all the components must be examined, in a whole, at the same instant of time, leading to the need of a unique model for the complete structure. Each junction between arms has been accurately examined (also manually if necessary) and properly modeled. A modal analysis [15] of the whole structure has been carried out to obtain the mode shapes and frequencies of the articulated device. A critical value of frequency of 1,1 Hz was identified. It corresponds to the critical frequency of the second mode of vibration in bending on a horizontal plane. As shown in Figure 10, the mode shape configuration of the whole structure shows critical areas at the root of the fifth arm. Frequency analyses performed during experimental tests are shown in Figure 10 too, for the three strain gages of "*A*" rosette and the three strain gages of "*C*" rosette of the first arm at the highest pumping frequency (0,43 Hz) and for the three strain gages of rosettes "*D*" and "*E*" of the third arm at medium pumping frequency (0,37 Hz). All the time, in the experimental results, a frequency peak as a response to the almost periodic pumping loading can be always seen at about 0,37 Hz, for medium pumping frequency, and at about 0,43 Hz, for the highest pumping frequency. In both cases, a further very high peak can be found (both numerically and experimentally) at about 1 Hz. This peak

corresponds to 1,1 Hz for the third and fifth arms. Consequently, comparison of numerical results with experimental ones shows a striking correlation. In fact, as shown by the numerical analysis, 1,1 Hz seems to be the most dangerous frequency for the entire structure. It corresponds to a vibration mode on a horizontal plane, excited by the pumping loading. On the contrary, during the static analysis, maximum stresses appear to originate mainly from bending on a vertical plane, which is a loading action more intuitive to understand (just giving a first glance to the structure of the articulated device).

3. Conclusions and Future Developments

In this paper, a deep analysis to test an articulated device for pouring concrete has been undertaken. The five-arms assembly has been tested both under quasi-static and on-service conditions. The so tested device should be the upgrade of a four-arms device already existing and actually working. For this purpose, a methodology has been formulated and validated that combines numerical and experimental analysis to verify the structure at the most critical frequencies and in the most stressed areas, starting from a classic strain analysis formulation. The sequential steps of the experimental elaboration are: the measurement of surface strains with a strain gage rosette, the transformation of measured strains to principal strains, the conversion of principal strains to principal stresses. Each step in this procedure has its own characteristic error sources and limits of applicability, to be avoided by means of suitable corrections on the thermal output, transverse sensitivity, signal attenuation due to lead wire resistance. These quantities have been determined with a graphical approach, by means of Mohr’s strain circles, thus reducing the strains measured on the rectangular rosette. Numerical technologies, especially the finite elements method, allow to simulate all the elements of the mechanical set with a very good precision, to simulate a large variety of load cases and to visualize in every point of the model the stress, the strain, the displacement. Numerical results have been confirmed by the experimental data, thus obtaining a high degree of correlation and a low deviation (from 5% to 7% as often as not): the calculus methodology is so

validated. The comparison between numerical and experimental results in on-service condition, at medium and high pumping speed, shows a very good correlation that allows to identify the more dangerous resonance frequencies for the structure (around 1 Hz). This frequency, which is the response to the forcing frequency of the pumping action, suggests that resonance is the more critical aspect to be checked in service for the apparatus. Therefore, the actual structural loadings cause negligible stresses if compared with the allowable strength of the Weldox 900 E steel use. This methodology approach, that combines numerical prediction and experimental tests, enhances the possibility for industries to collect and verify actual data of the structural resistance in the early phases of pre-production. The heavy mechanics industry field is characterized by products quantity far away from mass production numbers, so the early testing of products such as loading machines, earth-moving machines, forklift trucks, already in the prototyping phase become an important issue.

Further developments on this activity could concern:

- the study of the proper geometrical modification of the existing prototype and of its components, in terms of shape optimization;
- the evaluation of endurance predictions of the different mock-ups of this kind of articulated devices by means of numerical programs;
- the set-up of an out-of-service experimental testing rig for assessing the articulated device or its new models or upgrades, by simulating the actual working condition during concrete pumping activity.

Acknowledgement

Authors are very grateful to Ing. Paolo Proli for his support in this research activity.

References

[1] G. Malpensa, Dispositivo articolato per la deposizione del calcestruzzo: modellazione 3D, analisi MEF e confronto con i risultati sperimentali, First level

Mechanical Degree thesis (in Italian), 16 Gennaio 2009, Academic Tutor: G. Caligiana, 2009.

[2] R. Miralbés and L. Castejón, Design and Optimisation of Crane Jibs for Forklift Trucks, Proc. of the World Cong. on Engineering, London, U. K., Vol. II, 2009.

[3] D. Croccolo, M. De Agostinis and N. Vincenzi, Structural analysis of an articulated Urban bus chassis via FEM: a methodology applied to a case study, Strojniški Vestnik - Journal of Mechanical Engineering 57(11) (2011), 799. DOI:10.554.5/sv-jme.2011.077.

[4] M. Degidi, G. Caligiana, D. Francia, A. Liverani, G. Olmi and F. Tornabene, Strain gauge analysis of implant-supported, screw-retained metal frameworks: Comparison between different manufacturing technologies, Proceedings of the Institution of Mechanical Engineers, Part H: Journal of Engineering in Medicine June 23 (2016), DOI:10.1177/0954411916653623, (Published online before print).

[5] L. L. Martinez, A. F. Blom, C. H. Trogen and T. Dahle, Fatigue behaviour of steels with strength levels between 350 and 900 MPa influence of post weld treatment under spectrum loading, Proc. of the North European Engineering and Science Conf. (NESCO), Stockholm, Sweden, 1997.

[6] B. Brüderlin and D. Roller, Geometric Constraint Solving and Applications. Springer-Verlag, Berlin Heidelberg, Printed in Germany, 3-540-64416-4 (1998), 301.

[7] O. C. Zienkiewicz, R. L. Taylor and J. Z. Zhu, The Finite Element Method, Elsevier Butterworth-Heinemann, Linacre House, Jordan Hill, Oxford, OX2 8DP, 30 Corporate Drive, Burlington, MA 01803, 2005, 719 p.

[8] R. D. Cook, Finite Element Modeling for Stress Analysis, John Wiley & Sons, Inc., 1995, 315p.

[9] S. Moaveni, Finite Element Analysis Theory and Application with Ansys, Pearson, Prentice Hall, Inc., Upper Saddle River, New Jersey, 2003, 822p.

[10] T. Stolarski, Y. Nakasone and S. Yoshimoto, Engineering Analysis with Ansys Software, Elsevier Butterworth-Heinemann, Linacre House, Jordan Hill, Oxford, OX2 8DP, 30 Corporate Drive, Burlington, MA 01803, 2006, 456p.

[11] Measurements Group, Inc., Transverse Sensitivity Errors, Tech Note, TN-509 Micro Measurements Group, Raleigh, NC, USA, 1993.

[12] J. W. Dally and W. F. Riley, Experimental Stress Analysis, College House Enterprises, 4th ed., LLC 5713 Glen Cove Dr. Knoxville, TN 37919-8611, (2005), 571p.

[13] ESAM Traveller Plus Measurement System, Technical Manual, 2000, 63p.

[14] A. J. Durelli, E. A. Phillips and C. H. Tsao, Introduction to the Theoretical and Experimental Analysis of Stress and Strain, McGraw-Hill Book Co., Inc., New York, 1958, 497p.

[15] R. W. Clough and J. Penzien, Dynamics of Structures, McGraw Hill Book Co., International Edition, 1993, 738p.